Electron conditioning of technical surfaces at cryogenic and room temperature in the 0–1 keV energy range

Michal Haubner [a,b,*], Vincent Baglin [b], Bernard Henrist [b]

[a] Department of Physics, Faculty of Mechanical Engineering, Czech Technical University in Prague, Czech Republic
[b] European Organization for Nuclear Research (CERN), Geneva, Switzerland

ARTICLE INFO

ABSTRACT

In the superconducting magnets of the Large Hadron Collider (LHC) at CERN, most of the beam-induced heat load is intercepted by a beam-screen (BS) cryogenically cooled to 5–20 K. When circulating the bunched proton beam, an electron cloud (EC) can form and bombard the BS copper surface with high doses of predominantly low-energy electrons, which desorb gas and consequently increase the pressure. The beam-induced pressure rise decreases during operation as the electron irradiation diminishes the secondary electron yield (SEY) and the electron-stimulated desorption (ESD) yield, a phenomenon referred to as 'beam conditioning'. Low ESD and SEY values achieved rapidly are requisite to mitigate EC and maintain UHV in storage rings. We report data on ESD and SEY electron conditioning completed at cryogenic temperature with 0–1 keV electrons up to an electron dose of 5.10^{-3} C mm^{-2}. Our results show that SEY conditioning depends on the primary electron energy and also that ESD yield significantly decreases with temperature. At 15 K, the amorphous-carbon coating and laser-treated copper present SEY below 1.1 and have initial ESD yields 3–6 times lower than OFE copper. Our results conform to the SEY and ESD's general understanding and extend it towards cryogenic temperatures.

1. Introduction

The CERN's Large Hadron Collider (LHC) and other present or future cryogenic storage rings [1–6] develop an electron cloud (EC) when circulating a bunched particle beam. Inside the LHC beam-screen (BS) the circulating 7 TeV proton beam emits synchrotron radiation (SR) at critical energy of 44.1 eV [7], which irradiates the technical-grade copper surface of the BS and extracts photoelectrons [8,9]. These mostly low-energy electrons gain more energy from the electric wake-field behind passing proton bunches and impinge on the BS surface again while extracting secondary electrons. If the secondary electron yield (SEY) is sufficiently high, a positive feedback loop can form that is known as electron multipacting. The EC activity also leads to a pressure rise via electron stimulated desorption (ESD). High EC activity triggered by high SEY values imposes additional heat load on the BS cryogenic cooling, while high ESD yield values ultimately lead to a large dynamic pressure rise when circulating the proton beam. Hence, low values of ESD and SEY achieved in a short time of operation, are an imperative to maintain UHV conditions, to mitigate EC and to limit the heat load on cryogenics of storage ring. As a remedy, both the SEY and the ESD yield of the BS decrease to sufficiently low values when subjected to extended

electron irradiation, which is a commonly observed effect in LHC [10–13] and other accelerators [3,14–16]. In fact, dedicated beam-scrubbing runs were performed in the LHC to quickly reach high electron doses on the BS, leading to low SEY and ESD values that enable operating the machine at its full performance [17]. In-situ measurements performed at the LHC Vacuum Pilot Sector (VPS) by E. Buratin [18], as well as EC simulations by G. Iadarola [19], and other investigations [20], demonstrated that low-energy electrons below 20 eV dominate the EC energy spectrum with a minor peak of beam-accelerated electrons at few hundreds of eV. New accelerators operating at cryogenic temperature are designed with techniques in mind to mitigate the EC and the dynamic vacuum effect [21–23]. For the High-Luminosity LHC (HL-LHC) upgrade, novel low-SEY surface treatments are developed to effectively suppress electron multipacting leading to an EC formation and doing so also suppress the dynamic pressure rise caused by the ESD [24].

We present new ESD and SEY data measured at room and cryogenic temperatures for a technical-grade OFE copper in an as-received unbaked state cleaned for UHV by a warm ultrasonic isopropanol bath. The copper we used in this study closely represents the current state of the LHC beam-screen surface [8,9], which is made of an OFE

copper, colaminated onto a stainless-steel sheet and heat-treated under H_2 atmosphere. We didn't measure a notable difference between these two within our instrumental precision. This OFE copper surface serves as a baseline for comparing the two new low-SEY surface treatments studied for the HL-LHC: amorphous-carbon (a-C) coating [25] and laser-treated copper [26].

The amorphous-carbon was proven to lower the SEY below the EC multipacting limit, even at remarkably thin coverages [27]. We investigate the same 50 nm thin a-C coating that was recently deployed in one LHC quadrupole magnet during Long Shutdown 2. This is not to be confused with a much thicker version of 400 nm that was tested with LHC-type proton beams at CERN's SPS machine [28,29] and at cryogenic conditions inside the COLDEX experiment [30,31] and recently deployed in the CERN's SPS [32]. The samples tested here were created as witness samples when coating the COLDEX BS with a 50 nm a-C prior to installation for future tests in the framework of the HL-LHC upgrade.

The laser-treated surface was also successfully tested at cryogenic temperatures with LHC-type proton beams in the COLDEX [33,34]. The OFE copper samples investigated here were laser-treated with the following COLDEX-like parameters: 532 nm wavelength, 5 µJ pulse energy, 10 ps pulse duration, 240 pulses. s^{-1}, 200 kHz repetition rate, 13 µm beam width, 24 µm hatch distance, 10 mm s^{-1} scanning speed and under N_2 atmosphere. The laser settings indeed influence the resulting SEY, as reported [35], and presumably also the ESD. The same laser treatment also generates equally low SEY for stainless-steel and aluminium [26].

2. Material and methods

The experimental setup aims to reproduce in a controlled way the relevant HL-LHC conditions (UHV, temperature below 20 K, unbaked sample) of its cryogenic system and to study the ESD and SEY. Detailed technical description is given in a dedicated paper [63], so only briefly (see Fig. 1). At cryogenic temperatures, residual gases cryosorb on the cold surfaces, including the studied sample. Hence, the UHV is a must, corresponding to a Langmuir monolayer formation time in the order of few hours, giving enough time to study the intact surface. The pressure range of 10^{-10} mbar is achieved by a combination of a turbomolecular pump, a non-evaporable getter pump and a bakeout at 150 °C during 72 h. The µ-metal chamber houses a 4-axis cryomanipulator capable of cooling the studied flag-type sample down to 15 K by an open-cycle LHe cooling. Samples are inserted via a Load-lock, hence unbaked samples can be studied.
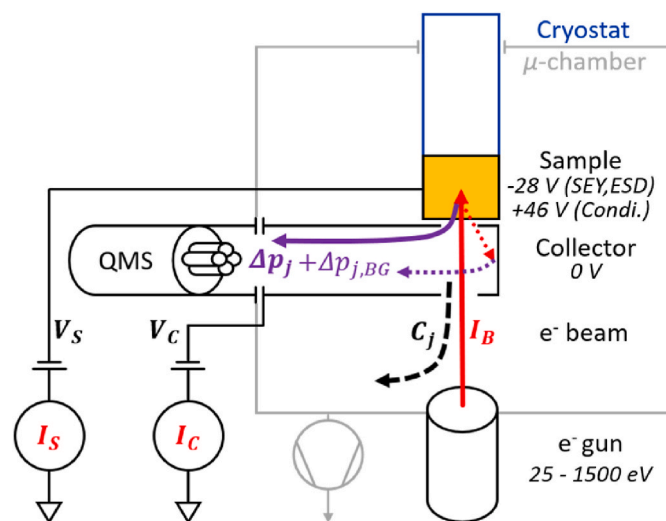

Fig. 1. Schematized arrangement for SEY and electron desorption measurements in the 0–1 keV region. See the text and Ref. [63]

Yet another experimental target is to reproduce the low-energy electron irradiation in the form of a monoenergetic slice of the electron cloud energy spectrum. This implies high accumulated doses, up to few mC.mm^{-2}, of low-energy electrons in the sub-keV range. A Kimball ELG-2 electron gun irradiates at a normal incidence the studied sample surface in a way that the EC in an accelerator would. The gun generates an electron beam with a low-energy (0–1.5 keV), low-intensity (0.1 nA - 10 µA), small spot size (3–7 mm^2) and with a flat-top profile, as measured by a Faraday-cup. A custom-designed collector is positioned 0.25 mm away from the sample and creates a closed geometry that captures the electrons and molecules that escape the studied sample as a result of the primary electron bombardment. The collector is spot-welded from stainless steel sheets, forming a geometry essentially consisting of a 75 mm wide and 750 mm long tube extending toward the QMS and an endcap with two 4 mm circular holes left for the primary electron beam to pass through the collector to the sample. Both the sample and collector are electrically floating, insulated by a sapphire plate and a ceramic interpiece, respectively, which allows measuring the electron currents and imposing a retarding sample bias. In addition, the collector acts as a Feulner cap [36] that protects the sample from any parasitic contamination originating from the setup and restricts the pumping speed to guide the desorbed gas molecules towards the quadrupole mass spectrometer (QMS) prior to being pumped. The conductance-limited pumping speed on the collector's inner volume, where the QMS is located, is invariably fixed by the geometry and does not change with the pumping speed inside the µ-chamber, that can vary. The pumping speed of the collector, with one hole covered by the sample, was calibrated against a known reference conductance by injecting gases alternately through this known conductance and into the collector. The measured conductance is 21.8 ℓ/s for H_2, with an uncertainty of 20%, and scales proportionally to $(2/M)^{1/2}$ for other gases of molecular mass M. This conductance is higher than expected for a 4 mm hole alone, because of gaps in the welded sheets. The collector is held at an ambient temperature, so the desorbing gases readily thermalize to 300 K, ruling out the need to correct for cryopumping and thermal transpiration. Meanwhile, the cryostat reaches ~5 K during a cooldown and the sample temperature remains around 15 K. The collector was redesigned since our last publication [37] towards a Feulner cap design, to mitigate gas recycling on the cold cryostat. Using this new experimental arrangement and methods, we measure the SEY and ESD yield of material surfaces as a function of energy and dose, at ambient and cryogenic temperatures, as follows.

Firstly, the Sample-Collector system acts as a Faraday cup that geometrically captures all the incoming electrons, as we have experimentally verified. The sum of collected currents equals the beam current $I_B = I_S + I_C$. This beam current I_B is then taken to calculate the SEY and ESD yield, as all these primary electrons do interact with the sample in some way. We set the sample bias to −28 V to measure the SEY and ESD as a function of primary electron energy. The low-energy electron beam in combination with the repulsive bias enables the energy sweep to start at 0 eV, as referenced to the sample. In this setting, the secondary electrons produced at the sample are repelled towards the grounded collector, where they form the collector current I_C. Dividing the collector current I_C by the beam current I_B gives the SEY, denoted δ, as follows:

$$\delta = I_{SE} / I_B = I_C / (I_S + I_C) \tag{1}$$

Secondly, the differentially pumped collector enables measuring the ESD yield $\eta_{e,j}$ of a gas species j as a result of primary electron irradiation of the studied sample. The yield is calculated from the calibrated vacuum conductance C_j of the collector and the pressure rise Δp_j, as measured by the in-situ calibrated QMS.

$$\eta_{e,j} = \frac{C_j.\Delta p_j}{k_B.T} \bigg/ \frac{I_B}{q_e} + \frac{C_j.\Delta p_{j,BG}}{k_B.T} \bigg/ \frac{I_C}{q_e} \approx \frac{C_j.\Delta p_j}{k_B.T} \bigg/ \frac{I_B}{q_e} \tag{2}$$

The measured ESD yield of a gas species $\eta_{e,j}$ has two terms. The first

term corresponds to the gas desorption from the studied sample stimulated by the primary electron beam I_B. The second term represents the dynamic background stimulated by electron current I_C impinging on the molecular collector which itself is a source of electrodesorbed gas. The collector is made of a 0.1 mm stainless-steel sheet that was UHV-cleaned and baked to achieve low degassing [38], followed by an in-situ electron conditioning. Hence, this dynamic background, captured by the second term, is generally much lower than the first term that comes from the high-yielding as-received sample under investigation. The static background from the residual gas is subtracted, as expressed by the Δp_j term in Equation (2). However, the dynamic background is not subtracted and its level is visible in the 0–10 eV range of Fig. 4. When measuring the ESD yield conditioning in Figs. 5 and 6, we use a $+46$ V sample bias to further minimize the dynamic background by attracting the secondary electrons back to the sample (in this case, the beam current I_B is still calculated as a sum of $I_S + I_C$, but SEY cannot be measured). The dynamic background level measured in Fig. 4 is used to remove the dynamic background from the data in Figs. 5 and 6.

The ESD yield is monitored for H_2, CO, CO_2, CH_4, C_2H_6, which are the main gases desorbing as a direct result of electron irradiation. The energy dependence is measured on the same spot and acquired point by point, increasing the primary electron energy, as seen in Figs. 2 and 3 for the SEY and Fig. 4 for the ESD yield. The energy step is set to 1 eV and 0.25 eV for ESD and SEY energy sweep, respectively, to capture the detailed dynamics of the low-energy region. This energy step is then spaced further apart, to minimize the electron dose imposed on the studied surface. In an SEY energy sweep, the beam current of 0.3 nA integrates to a dose of 10^{-8} C mm^{-2}, making the SEY measurement a non-destructive routine. For an ESD curve, a similar energy sweep is done with a µA beam current that integrates to a few 10^{-5} C mm^{-2}. Although this current is received mostly at low energy, measuring ESD is destructive by definition, as some molecules are removed from the studied surface. Indeed during an ESD energy sweep, we observe a conditioning effect of a few tens of percent. A smoothed curve is fitted into the data to guide the eye by capturing the trend behind the scattered datapoints.

The conditioning effect achieved by extended electron irradiation can be measured at room and cryogenic temperature, as shown in Fig. 5, which plots the ESD yield against the accumulated electron dose. The same irradiation with 300 eV primary electrons is done at 260 K and 15 K for comparison. Fig. 6 shows the ESD yield conditioning curves of low-SEY surface treatments under 300 eV electron irradiation at 15 K.

The setup enables the study of SEY and ESD yields of material samples as a function of energy and dose. We typically measure the SEY and ESD energy dependence of an as-received surface state of each studied sample. Then, another intact spot is chosen on the same sample that is irradiated with electrons at a given energy. We chose the 300 eV primary energy as a baseline as it provides the most effective conditioning effect. During this irradiation, the ESD yield of the main gas species is measured and plotted as a function of the impinging electron dose. At last, another SEY curve is measured on the conditioned surface to describe the final surface state. The SEY measurement is also used to reference the primary electron energy scale with respect to the sample. Thereby, all electron energies are taken with respect to this vacuum level E_{vac}, as localized by the inflection point of the work function edge of the sample.

3. Results and discussion

3.1. SEY measurements

Using this experimental method, we have measured the effect of SEY conditioning for various surfaces held at 15 K. The effect of varying primary electron energy is illustrated on an OFE copper. The surface state of an as-received unbaked OFE copper that we studied featured a maximum SEY, $\delta_{max} = 2.8$, peaking around 300 eV. The presence of contaminants on the intact surface not only manifests by a large δ_{max}, but is also evidenced by the presence of ~7 eV peak visible in the inset of the left graph on Fig. 2. Electron conditioning was then done for three different primary electron energies. The 300 eV electrons at a dose of 2.3 mC mm^{-2} condition the δ_{max} to 1.1 and shift the peak towards 200 eV. Conditioning with 1 keV electrons at the same dose achieves almost the same conditioning effect. This conditioning process is well understood and described at ambient temperatures [39–41]. The low SEY and peak around 200 eV is assigned to precipitation of graphitic carbon overlayer on the copper surface. Conversely, 23 eV electrons do not condition the SEY nearly as well as, not even at twice the dose. The δ_{max} does not decrease below 1.45 and the peak does not shift towards 200 eV. Such limited conditioning effect that low-energy electrons have on copper was also measured by Refs. [39,42], in these cases at room temperature, and was linked to the lack of surface carbonization.

The right graph in Fig. 3 shows the SEY conditioning effect measured for the case of 50 nm thick a-C coating and for laser-treated copper surface, both of which are in an as-received unbaked state and held at 15 K. Both surface treatments are designed to have intrinsically low SEY [25,26] well below the LHC multipacting limit of $\delta_{max} = 1.35$ in dipoles (or 1.1 in quadrupoles) for 6.5 TeV protons beams [43].

The data show that the SEY is further reduced by 300 eV electron irradiation. When exposed to an electron dose of 4 mC mm^{-2}, the δ_{max} of a-C drops from 1.15 to 0.85 and the peak shifts closer towards 200 eV, corresponding to the lack of contaminants on the graphitic surface. This
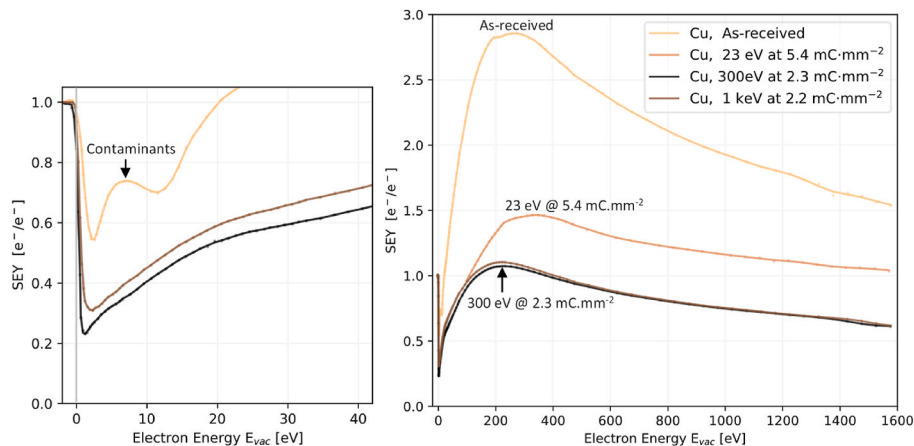

Fig. 2. SEY curves of OFE Cu measured at 15 K as a function of primary electron kinetic energy, which is referenced to the vacuum level of the sample. Left graph zooms into the low-energy region and shows the contaminant removal and surface graphitization.
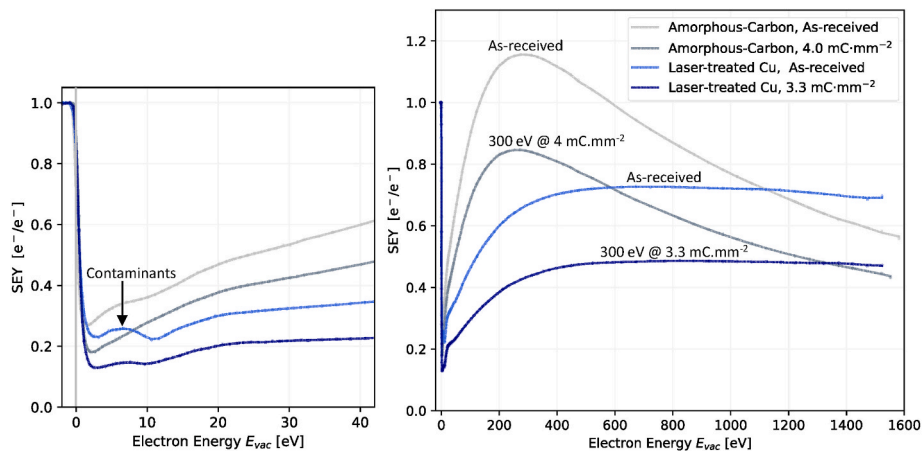
Fig. 3. SEY curves measured at 15 K as a function of primary electron kinetic energy, referenced to the sample vacuum level. The SEY curves for 50 nm amorphous-carbon and laser-treated copper show the as-received and conditioned states.
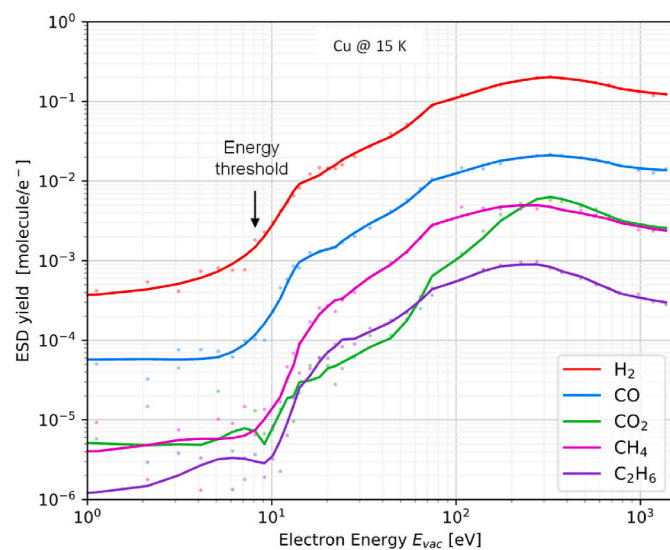

Fig. 4. ESD yield as a function of primary electron energy, as measured for an unbaked as-received OFE copper at 15K. The energy threshold is marked by an arrow around 10 eV and is similar for all chemisorbed gases. Below this threshold lies the collector's dynamic background signal, which is highest for H_2 and CO.

corresponds to results obtained for amorphous-carbon in an as-received state with the δ_{max} in the 1.15 to 0.85 range. The obtained δ_{max} was demonstrated to vary with the surface state, achieved by specific coating process parameters, storage methods and thermal treatments [25, 44–46].

Owing to its microgeometry, the laser-treated copper surface exhibits a characteristically flat SEY curve with only a flat peak and intrinsically low δ_{max} [35,47–49]. We measured that the δ_{max} further decreases, from 0.73 to 0.5, when irradiated with 300 eV electrons at a dose of 3.3 mC mm^{-2}. The overall decrease can again be ascribed to the electron-stimulated removal of surface contaminants, as evidenced by the reduction of the 7 eV peak. Likewise the bare copper and a-C coating, the general shape of the SEY curve does not evolve during an e$^-$ conditioning, but only scales down towards lower SEY values.

It is remarkable to note that cooling down both studied low-SEY treatments to a cryogenic temperature does not strongly modify the δ_{max} as compared to room temperature studies [25,50]. Our data for laser-treated copper agree with SEY measurements done at cryogenic temperatures [51].

3.2. ESD yield as a function of primary electron energy

Similarly to the SEY, the ESD yield can also be measured as a function of energy, as illustrated in Fig. 4. The ESD signal only consists of the dynamic background in the 1–10 eV energy region. As the primary energy ramps up, the signal from the studied sample eventually surpasses the dynamic background level and rapidly becomes the predominant gas source. We interpret this discontinuity to be the desorption energy
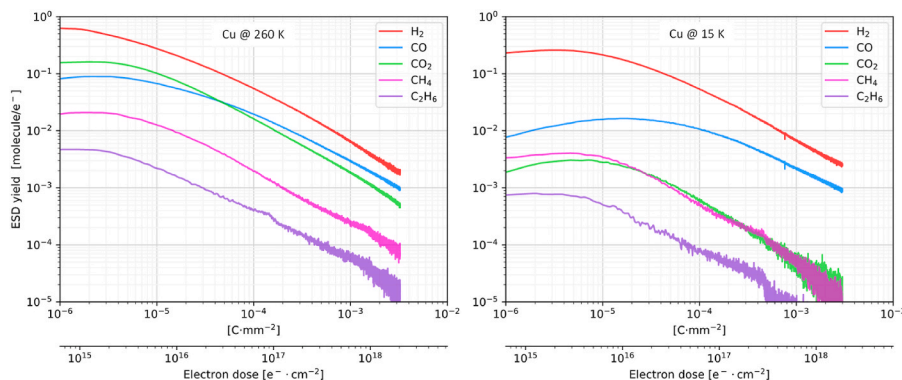

Fig. 5. ESD conditioning curves measured for OFE copper held at 260 K (left) and 15 K (right).
The copper surface in an unbaked as-received surface state was irradiated with 300 eV electrons.
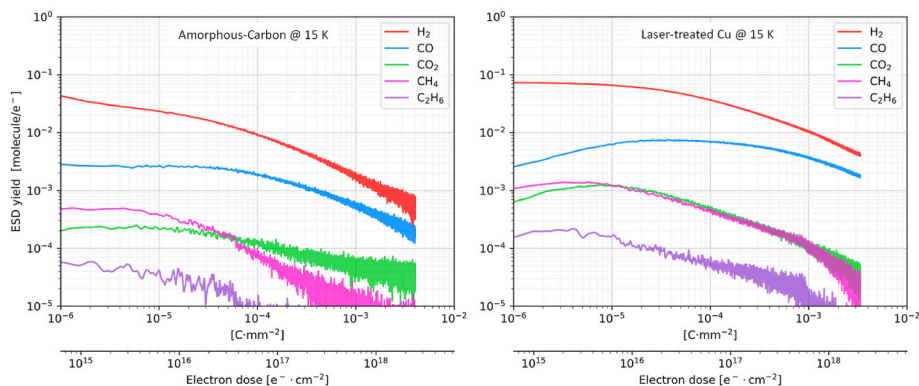
Fig. 6. ESD conditioning curves measured for 50 nm amorphous-carbon (left) and laser-treated (right) copper surface. The studied surfaces are unbaked, as-received, held at 15K and conditioned with 300 eV electrons.

threshold, as described in the framework of the classical IMGR model, developed independently by Ishikawa [52], Menzel & Gomer [53] and Redhead [54]. This is remarkably close to the 10 eV effect mentioned in Redhead's memoirs [55] and the values extrapolated by Billard et al. for room temperature OFHC copper [56]. As much as the data scatter and dynamic background allows us to draw conclusions, the energy threshold is similar for all monitored gases and lies below 10 eV. Beyond this energy threshold, the ESD yield increases linearly due to the primary electron energy being deposited within the secondary electrons (SE) escape depth. The yield reaches a flat peak at a few hundreds of eV and is followed by a slow decrease. This decrease at higher energies is partly due to electron conditioning done during the energy sweep itself and partly due to the primary e^- depositing energy deeper within the bulk, in a depth comparable to the SE escape depth. The ESD yield of all monitored gases follows a similar trend across the entire energy range.

3.3. ESD conditioning

Extended electron irradiation decreases the ESD yield of all desorbing gas species, i.e. H_2, CO, CO_2, CH_4, C_2H_6, in an effect called conditioning. Subjecting a surface to a continuous 300 eV electron irradiation desorbs molecules, depletes their surface coverage and decreases the ESD yield. The ESD yield can be plotted as a function of accumulated e^- dose, as illustrated in Fig. 5 for unbaked copper at 260 K and 15 K. Fig. 6 shows 300 eV conditioning for amorphous carbon and laser-treated copper both unbaked and held at 15 K.

In the ambient temperature case, the conditioning curve of an ESD yield for all species typically starts with a plateau which holds the initial ESD yield for about a decade of electron dose until a few 10^{15} $e^-.cm^{-2}$. A steady decrease then follows at higher doses. The conditioning rate asymptotically approaches a constant decline that can be fitted by an inverse power law with an exponent typically in the 0.5–1 range. The conditioning rate approaches a slope of 1 for copper at ambient and cryogenic temperature. The ESD yields of CH_4, C_2H_6 and CO_2 and by extension their conditioning rates are less conclusive at high electron doses, as we are approaching the sensitivity limit of the experimental setup.

The ESD yield of all monitored gas species behaves differently, when comparing the ambient temperature to the copper at 15 K. The cryogenic temperature causes the initial yield to decrease, presumably due to lower recombination rate/mobility on the surface or diffusion in the bulk. The initial H_2 yield is the least affected and drops only by a factor of 4. The initial yield of CH_4, C_2H_6 and CO decreases by a decade, whilst the CO_2 yield drops by almost two decades. The formation of CO_2 on the surface and a subsequent desorption seems very ineffective at 15 K for all the studied surfaces. By contrast, the H_2 and CO yields, approach their room temperature counterpart at high electron doses.

The CO and CO_2 yields exhibit a transient maximum before starting a steady decrease. We ascribe this maximum to the fact that at 15 K, we measure a recycling ESD yield in our conductance-limited collector. Hence, the measured signal is a superposition of the primary desorption and secondary desorption of gases cryosorbed into a sub-monolayer coverage, similarly to the case studied in Refs. [57,58]. Indeed, we observe vacuum transients similar to the above references where the upper-limit of the recycling yield is given by the quasi-static gas density in the collector, that is determined by the ratio of the collector conductance to the cryo-sample pumping speed. In our case, this upper limit value equals 2. Hence, the initial ESD yield we measure in our experimental arrangement can only be underestimated by a factor of 2.

The same measurement of ESD yield conditioning was performed on a 50 nm amorphous-carbon and the laser-treated copper, both held at 15 K while irradiated with 300 eV electrons. The a-C exhibits an initial ESD yield lower by a factor of 3–6, as compared to copper at 15 K. There is no transient maximum and after the initial plateau, the ESD yield declines for all gas species. Similarly to the a-C, the laser-treated copper exhibits lower initial ESD yields. However, a transient maximum is observed, especially for CO and CO_2, this time at a higher electron dose than for copper, which can be linked to the large specific surface.

Table 1 gives the ESD yields for different stages of the conditioning process and serves to compare the a-C and laser-treated sample against bare OFE copper at 15 K. For clarity, we focus on H_2 and CO as the predominant desorbing gases. The copper at 260 K is used to substantiate the different behaviour of ESD yield evolution with electron dose at ambient and cryogenic temperatures.

When comparing the a-C and laser-treated samples against the bare copper at 15 K, they exhibit overall lower initial ESD yields. In fact, the as-received copper at 15 K requires a dose of 10^{17} $e^-.cm^{-2}$ to reach the same H_2 yield as amorphous-carbon has ab-initio. At a dose of 10^{18} e^-.cm^{-2}, the copper conditions to similar ESD yields as the laser-treated surface, but the a-C already has by almost a decade lower ESD yields. The reduction of H_2 and CO yields can be calculated between doses of 10^{17} and 10^{18} $e^-.cm^{-2}$. The copper surface, regardless of the temperature, reduces its ESD yields by a factor of 5.5–10 per decade of electron dose. This is a characteristic observation for a clean metal surface, where the decrease approaches a factor of 10. By contrast, both surface treatments reduce their ESD yield at about half the rate, even at high e^- doses. Hence the electron conditioning seems less effective here and is likely linked to the surface porosity.

The integral amount of gas desorbed during a conditioning can also be evaluated. For an electron dose of 10^{17} $e^-.cm^{-2}$, there are only marginal differences in the H_2 and CO desorbed from copper, regardless of temperature, and including the laser-treated copper. The desorbed gas corresponds to 5–11 .10^{15} molecules. cm^{-2} for H_2 and 0.7–3 .10^{15} molecules. cm^{-2} for CO. At the same electron dose, the amorphous-carbon desorbs about 6 times less H_2 and CO than bare copper at 15 K.

Table 1

Comparison of H_2 and CO yields of the studied surfaces as sampled at the initial as-received surface state and at doses of 10^{17} $e^-.cm^{-2}$ and 10^{18} $e^-.cm^{-2}$ during the 300 eV conditioning.

	OFE Cu at 260 K		OFE Cu at 15 K		50 nm a-C/Cu at 15 K		Laser-treated Cu at 15 K	
	H_2	CO	H_2	CO	H_2	CO	H_2	CO
Initial Yield [molecule/e^-]	6.2E-1	8.3E-2	2.3E-1	7.9E-3	4.1E-2	2.8E-3	7.4E-2	2.7E-3
Yield at 10^{17} $e^-.cm^{-2}$ [molecule/e^-]	3.7E-2	1.4E-2	3.7E-2	8.4E-3	7.0E-3	1.5E-3	3.0E-2	6.5E-3
Yield at 10^{18} $e^-.cm^{-2}$ [molecule/e^-]	3.8E-3	1.9E-3	4.4E-3	1.5E-3	1.1E-3	4.0E-4	7.4E-3	2.9E-3
Reduction factor in 10^{17}-10^{18} $e^-.cm^{-2}$ [-]	9.8	7.1	8.4	5.6	6.6	3.8	4.0	2.3
Desorbed gas at 10^{17} $e^-.cm^{-2}$ [mbar.l.cm^{-2}]	4.5E-4	1.2E-4	3.7E-4	5.1E-5	5.7E-5	9.1E-6	1.9E-4	3.0E-5

4. Conclusions

We have developed and validated a methodology for measuring SEY and ESD yield at cryogenic temperatures and in the low-energy range of 0–1 keV. The new setup produces data in excellent agreement with values found in literature taken under similar parameters. This includes the SEY measured at ambient [40] and cryogenic temperatures [59] and of ESD yields and conditioning rates measured at ambient temperature [56,60,61] as well as the effect that varying primary electron energy has on the SEY conditioning process [39]. We first studied an OFE copper representing the LHC beam-screen to establish a reference at both ambient and cryogenic temperatures. We then proceeded with studies of novel low-SEY surface treatments to directly compare their SEY, ESD yields and electron conditioning effects.

We report the first laboratory measurements of electron conditioning of both SEY and ESD yield performed at a cryogenic temperature of 15 K. We showed that the primary electron energy has a major influence on the SEY conditioning efficiency. We evidence this by incomplete SEY conditioning when irradiating the OFE copper with 5.4 mC mm^{-2} of 23 eV electrons that only resulted in $\delta_{max} = 1.45$. This is to be compared to the full conditioning effect, i.e. $\delta_{max} = 1.1$, achieved by exposing copper to 300 eV electrons at a dose of 2.3 mC mm^{-2}. The lack of conditioning efficiency of low-energy e^- was previously demonstrated for copper at room temperature [39], and we evidence this effect at cryogenic conditions. Our results complement the existing data on SEY conditioning measured in the cryogenic temperature region by Cimino & Collins [59]. Here we further investigate the effect of primary electron energy on the OFE copper conditioning.

The ESD yield from OFE copper at 15 K was also studied as a function of primary e^- energy, revealing a ~10 eV threshold, below which the electron-stimulated desorption yield is nil. This observation compares well to the values extrapolated by Billard et al. [56] for as-received OFHC copper at ambient temperature. The energy dependence of ESD is linear for all monitored gases until reaching a flat peak at a few hundreds of eV. Unlike for the SEY conditioning which is rather temperature-independent, the ESD yields are substantially lower for copper at 15 K. The cryogenic conditions lead to about a decade lower initial ESD yield for CH_4, C_2H_6 and CO, whilst the initial H_2 yield drops by a factor of ~3 and the initial CO_2 yield decreases by 2 decades. The ESD conditioning curves also exhibit a very different behaviour at cryogenic temperatures, when compared to copper ambient temperatures. The CH_4, C_2H_6 and CO_2 yields remain lower at high electron doses. By contrast, the H_2 and CO yields ultimately converge to the values obtained for a room temperature copper. The conditioning rate at high electron doses remains unchanged at 15 K and approaches a slope of 1 for copper and about half of that for the studied low-SEY treatments.

We also report the first results taken at cryogenic temperatures on electron conditioning of HL-LHC-relevant low-SEY surface treatments. We demonstrate across the studied energy range that both surface treatments preserve their low δ_{max} even at cryogenic temperatures. Indeed, the SEY of as-received unbaked amorphous-carbon (50 nm) and laser-treated copper do remain well below the multipacting threshold for LHC cryodipole, i.e. $\delta_{max} < 1.3$. The SEY further decreases when exposed to 300 eV electron irradiation at 15 K. The δ_{max} of amorphous-

carbon conditions from 1.15 to 0.85 at a dose of 4 mC mm^{-2}, whilst δ_{max} of laser-treated copper conditions from 0.73 to 0.5 at a dose of 3.3 mC mm^{-2}.

The initial ESD yields of both low-SEY surface treatments are lower than of an as-received unbaked OFE copper. The ESD yield of copper only conditions to comparable ESD values at an electron dose of few 10^{-4} C mm^{-2}. Compared to the copper, the amorphous-carbon coating lower by almost a decade at an electron dose of few mC.mm^{-2}. Contrary to the copper surface, both amorphous-carbon and laser-treated copper exhibit a slower ESD conditioning rates that approach a slope of 0.5 rather than 1. The conditioning curves produced at a cryogenic temperature do complement the observations made by Hannah et al. for a laser-treated copper at ambient temperature [62]. The conditioning rates at high electron doses are similar to Hannah's, but the initial yields are overall lower at 15 K, which is expected knowing the substantial decrease of copper ESD yields in Fig. 5.

The presented experimental results link the e^- cloud activity, the dynamic vacuum effect and the beam conditioning, all observed in the LHC's cold arcs. These new insights into the LHC vacuum system are especially relevant with the HL-LHC upgrade under way [24]. The data can also serve other cryogenic machines [3] and provide an input for design and simulations of new accelerators, such as the FCC-hh [5,23].

CRediT authorship contribution statement

Michal Haubner: Writing – review & editing, Writing – original draft, Visualization, Software, Methodology, Investigation, Data curation. **Vincent Baglin:** Writing – review & editing, Supervision, Resources, Project administration, Funding acquisition, Formal analysis. **Bernard Henrist:** Supervision, Methodology, Formal analysis, Data curation, Conceptualization.

Declaration of competing interest

The authors declare that they have no known competing financial interests or personal relationships that could have appeared to influence the work reported in this paper.

Data availability

Data will be made available on request.

Acknowledgements

References

[1] G. Rumolo, N. Mounet, C. Zannini, Arduini, et al., Electron cloud observations in LHC (No. CONF, in: Proc. of IPAC'11, Sept 2011, San Sebastian, Spain, 2011, pp. 2862–2864. URL: jacow.org/IPAC2011/papers/THOBA01.pdf.

[2] G. Iadarola, G. Rumolo, G. Arduini, H. Bartosik, et al., Electron Cloud and Scrubbing Studies for the LHC (No. CERN-ACC-2013-0054), in: Proc. Of IPAC'13, May 2013, Shanghai, China, 2013. URL: cds.cern.ch/record/1572988.

[3] W. Fischer, M. Blaskiewicz, M. Brennan, H. Huang, et al., Electron cloud observations and cures in the relativistic heavy ion collider, Phys. Rev. ST Accel. & Beams 11 (2008), 041002, https://doi.org/10.1103/PhysRevSTAB.11.041002.

[4] C. Montag, V. Ptitsyn, eRHIC in ICFA Beam Dynamics Newsletter No. 74, E Gianfelice-Wendt, August 2018.

[5] M. Benedikt, et al., FCC-Hh: the hadron collider, Eur. Phys. J. Spec. Top. 228 (4) (2019) 755–1107, https://doi.org/10.1140/epjst/e2019-900087-0.

[6] The CEPC-SPPC Study Group, CEPC-SppC Preliminary Conceptual Design Report, Vol vol. II: Accelerator, IHEP-CEPC-DR-2015-01, March 2015. URL: cepc.ihep.ac.cn/preCDR/Pre-CDR_final_20150317.pdf.

[7] Baglin, V., Bregliozzi, G., Lanza, G., Jimenez, J. M. Synchrotron radiation in the LHC vacuum system, Proc. Of IPAC'11, September 2011, San Sebastian, Spain. URL: cds.cern.ch/record/1407539.

[8] O. Brüning, et al., LHC Design Report, CERN-2004-003, Geneva, Switzerland, June 2004, https://doi.org/10.5170/CERN-2004-003-V-2.

[9] O. Gröbner, Overview of the LHC vacuum system, Vacuum 60 (1–2) (2001) 25–34, https://doi.org/10.1016/S0042-207X(00)00240-2.

[10] G. Bregliozzi, V. Baglin, P. Chiggiato, P. Cruikshank et al. Observations of electron cloud effects with the LHC vacuum system, Proc. of IPAC'11, September 2011, San Sebastian, Spain. paper TUPS018, pp. 1560-1562. URL: jacow.org/IPAC2011/papers/TUPS018.pdf.

[11] G. Lanza, V. Baglin, G. Bregliozzi, J. M. Jimenez. LHC Beam vacuum during 2011 machine operation, Proc. Of IPAC'12, May 2012, New Orleans, Louisiana, USA. URL: jacow.org/IPAC2012/papers/WEPPD018.pdf.

[12] G. Lanza, V. Baglin, G. Bregliozzi, J. M. Jimenez. LHC vacuum system: 2012 review and 2014 outlook, Proc. Of LHC Beam Operation Workshop - Evian 2012, December 2012, CERN-ATS-2013-045, Geneva, Switzerland. URL: cds.cern.ch/record/2302432.

[13] Baglin, V., Bregliozzi, G., Lanza, G., & Jimenez, J. M. Vacuum performance and lessons for 2012, Proc. Of Chamonix 2012 Workshop on LHC Performance, CERN-2012-006, Geneva, Switzerland. DOI: 10.5170/CERN-2012-006.74.

[14] S.Y. Zhang, L. Ahrens, J. Alessi, M. Bai, et al., Experience in reducing electron cloud and dynamic pressure rise in warm and cold regions in RHIC, in: Proc. Of EPAC 2006, June 2006. Edinburgh, Scotland. URL: www.osti.gov/biblio/885019.

[15] Y. Suetsugu, K. Kanazawa, S. Kato, et al., Present status of the KEK B-factory vacuum system, J. Vac. Sci. Technol., A 21 (2003) 1436, https://doi.org/10.1116/1.1577129.

[16] Y. Suetsugu, K. Shibata, T. Ishibashi, et al., Achievements and problems in the first commissioning of superKEKB vacuum system, J. Vac. Sci. Technol., A 35 (2017), 03E103, https://doi.org/10.1116/1.4977764.

[17] V. Baglin, The LHC vacuum system: commissioning up to nominal luminosity, Vacuum 138 (2017) 112–119, https://doi.org/10.1016/j.vacuum.2016.12.046.

[18] E. Buratin, Electron Cloud and Synchrotron Radiation Characterization of Technical Surfaces with the Large Hadron Collider Vacuum Pilot Sector (Doctoral dissertation, CERN), 2020. EPFL. URL: cds.cern.ch/record/2746058.

[19] G. Iadarola, Electron Cloud Studies for CERN Particle Accelerators and Simulation Code Development, Doctoral dissertation, CERN, 2014. URL: cds.cern.ch/record/1705520.

[20] R. Cimino, T. Demma, Electron cloud in accelerators, Int. J. Mod. Phys. 29 (No.17) (2014), 1430023, https://doi.org/10.1142/S0217751X14300233.

[21] S.Y. Zhang, eRHIC Beam Scrubbing, BNL-114220-2017-IR, Brookhaven National Laboratory, Upton, NY, United States, June 2017, https://doi.org/10.2172/1392223.

[22] G. Rumolo, I. Hofmann, E. Mustafin, O. Boine-Frankenheim, Vacuum and electron cloud issues at the GSI present and future facilities, in: Proc. Of ECLOUD'04: 31st Advanced ICFA Beam Dynamics Workshop on Electron-Cloud Effect, 2005, pp. 95–101, https://doi.org/10.5170/CERN-2005-001.95. Napa, CA, USA.

[23] I. Bellafont, M. Morrone, L. Mether, J. Fernández, et al., Design of the future circular hadron collider beam vacuum chamber, Physical Review Accelerators and Beams 23 (3) (2020), 033201, https://doi.org/10.1103/PhysRevAccelBeams.23.033201.

[24] High-Luminosity Large Hadron Collider (HL-LHC): Technical Design Report Ed. by I. Bejar Alonso, O. Brüning, P. Fessia, M. Lamont, L. Rossi, L. Tavian, M. Zerlauth. CERN 2020-10, CERN, Geneva, Switzerland. DOI: 10.23731/CYRM-2020-0010.

[25] P.C. Pinto, S. Calatroni, H. Neupert, D. Letant-Delrieux, et al., Carbon coatings with low secondary electron yield, Vacuum 98 (2013) 29–36, https://doi.org/10.1016/j.vacuum.2013.03.001.

[26] R. Valizadeh, O.B. Malyshev, S. Wang, Zolotovskaya, et al., Low secondary electron yield engineered surface for electron cloud mitigation, Appl. Phys. Lett. 105 (23) (2014), 231605, https://doi.org/10.1063/1.4902993.

[27] M. Angelucci, A. Novelli, L. Spallino, Liedl, et al., Minimum thickness of carbon coating for multipacting suppression, Physical Review Research 2 (3) (2020), 032030.

[28] C.Y. Vallgren, P. Chiggiato, P.C. Pinto, H. Neupert, et al., Performance of carbon coating for mitigation of electron cloud in the SPS, in: Proc. 2nd Int. Particle Accelerator Conf.(IPAC'11), 2011, pp. 1590–1592, https://doi.org/10.1103/PhysRevResearch.2.032030.

[29] M. Van Gompel, P. Chiggiato, P.C. Pinto, P. Cruikshank, et al., Amorphous carbon thin film coating of the SPS beamline: evaluation of the first coating implementation, in: 8th Int. Particle Accelerator Conf. (IPAC'17), May 2017, Copenhagen, Denmark, 2017, May, https://doi.org/10.18429/JACoW-IPAC2017-MOOCA3.

[30] Salemme, R., Baglin, V., Bregliozzi, G., Chiggiato, P et al. Amorphous carbon coatings at cryogenic temperatures with LHC type beams: first results with the COLDEX experiment, Proc. Of IPAC'15, May 2015, Richmond, Va, USA. URL: cds.cern.ch/record/2141874.

[31] R. Salemme, V. Baglin, G. Bregliozzi, P. Chiggiato, Vacuum performance of amorphous carbon coating at cryogenic temperature with presence of proton beams, in: Proc. Of IPAC'16, May 2016, https://doi.org/10.18429/JACoW-IPAC2016-THPMY007. Busan, Korea.

[32] Amorphous carbon coating in SPS, W. Vollenberg, et al., Proc. Of IPAC'21, virtual ed, September 2021, https://doi.org/10.18429/JACoW-IPAC2021-WEPAB338. Campinas, Brazil.

[33] R. Salemme, V. Baglin, S. Calatroni, P. Chiggiato, et al., First beam test of Laser Engineered Surface Structures (LESS) at cryogenic temperature in CERN SPS accelerator, in: Journal of Physics: Conference Series, vol. 1067, IOP Publishing, 2018, September, 082017, https://doi.org/10.18429/JACoW-IPAC2018-WEPMG005, 8.

[34] Baglin, V. COLDEX: a tool to study cold surfaces in accelerators, Proceedings of ECLOUD'18, June 2018, Isola d'Elba, Italy. CERN-2020-09-19, Geneva, Switzerland. DOI: 10.23732/CYRCP-2020-007.165.

[35] D. Bajek, S. Wackerow, D.A. Zanin, L. Baudin, et al., Role of surface microgeometries on electron escape probability and secondary electron yield of metal surfaces, Sci. Rep. 10 (1) (2020) 1–8, https://doi.org/10.1038/s41598-019-57160-w.

[36] P. Feulner, D. Menzel, Simple ways to improve" flash desorption" measurements from single crystal surfaces, 1980, https://doi.org/10.1116/1.570537.

[37] R. Dupuy, M. Haubner, B. Henrist, J.H. Fillion, V. Baglin, Electron-stimulated desorption from molecular ices in the 0.15-2 keV regime, J. Appl. Phys. 128 (17) (2020), 175304, https://doi.org/10.1063/5.0021832.

[38] V. Nemanič, J. Šetina, Outgassing in thin wall stainless steel cells, J. Vac. Sci. Technol.: Vacuum, Surfaces, and Films 17 (3) (1999) 1040–1046, https://doi.org/10.1116/1.581680.

[39] R. Cimino, M. Commisso, D.R. Grosso, T. Demma, et al., Nature of the decrease of the secondary-electron yield by electron bombardment and its energy dependence, Phys. Rev. Lett. 109 (6) (2012), 064801, https://doi.org/10.1103/PhysRevLett.109.064801.

[40] M. Nishiwaki, S. Kato, Graphitization of inner surface of copper beam duct of KEKB positron ring, Vacuum 84 (5) (2009) 743–746, https://doi.org/10.1016/j.vacuum.2009.06.028.

[41] C. Scheuerlein, M. Taborelli, N. Hilleret, A. Brown, M.A. Baker, An AES study of the room temperature conditioning of technological metal surfaces by electron irradiation, Appl. Surf. Sci. 202 (1–2) (2002) 57–67, https://doi.org/10.1016/S0169-4332(02)00868-1.

[42] R. Larciprete, D.R. Grosso, M. Commisso, R. Flammini, et al., Secondary electron yield of Cu technical surfaces: dependence on electron irradiation, Phys. Rev. Spec. Top. Accel. Beams 16 (1) (2013), 011002, https://doi.org/10.1103/PhysRevSTAB.16.011002.

[43] G. Iadarola, A.P. Axford, G. Rumolo, H. Bartosik, K. Li, Effect of Electron Cloud in Quadrupoles on Beam Instability, Proc. of. IPAC'15, Richmond, VA, USA, May 2015, https://doi.org/10.18429/JACoW-IPAC2015-MOPJE051.

[44] C.Y. Vallgren, A. Ashraf, S. Calatroni, P. Chiggiato, et al., Low secondary electron yield carbon coatings for electron cloud mitigation in modern particle accelerators, in: Proc. Of IPAC'10, May 2010, Kyoto, Japan., 2011 cds.cern.ch/record/1309161.

[45] A. Ashraf, M. Mehmood, S.A. Janjua, Study of ultra-high-vacuum properties of carbon-coated stainless steel beam pipes for high-energy particle accelerators, Arabian J. Sci. Eng. 44 (7) (2019) 6593–6600, https://doi.org/10.1007/s13369-019-03761-6.

[46] H.M. Fernández, M. Himmerlich, P.C. Pinto, J. Coroa, Sousa, et al., The impact of H_2 and N_2 on the material properties and secondary electron yield of sputtered amorphous carbon films for anti-multipacting applications, Appl. Surf. Sci. 542 (2021), 148552, https://doi.org/10.1016/j.apsusc.2020.148552.

[47] M. Pivi, F.K. King, R.E. Kirby, T. Raubenheimer, et al., Sharp reduction of the secondary electron emission yield from grooved surfaces, J. Appl. Phys. 104 (10) (2008), 104904, https://doi.org/10.1063/1.3021149.

[48] Y. Wang, W. Zhang, S. Wang, W. Wei, et al., Influence of primary electron incident angle and electron bombardment on the secondary electron yield of laser-treated copper, Journal of Vacuum Science & Technology B, Nanotechnology and Microelectronics: Materials, Processing, Measurement, and Phenomena 39 (3) (2021), 034201, https://doi.org/10.1116/6.0000952.

[49] M. Ye, P. Feng, Y. Li, D. Wang, et al., The total secondary electron yield of a conductive random rough surface, J. Appl. Phys. 125 (4) (2019), 043301, https://doi.org/10.1063/1.5023769.

[50] R. Valizadeh, O.B. Malyshev, S. Wang, T. Sian, et al., Reduction of secondary electron yield for E-cloud mitigation by laser ablation surface engineering, Appl. Surf. Sci. 404 (2017) 370–379, https://doi.org/10.1016/j.apsusc.2017.02.013.

[51] S. Calatroni, E.G.T. Valdivieso, A.T.P. Fontenla, Taborelli, et al., Optimization of the secondary electron yield of laser-structured copper surfaces at room and cryogenic temperature, Physical Review Accelerators and Beams 23 (3) (2020), 033101, https://doi.org/10.1103/PhysRevAccelBeams.23.033101.

[52] K. Mase, A. Nambu, Pioneers of study on desorption induced by electronic transitions; achievements by dr. Yoshioki Ishikawa and dr. Yoshio ohta, Journal of

the Vacuum Society of Japan 49 (10) (2007) 610–617, https://doi.org/10.3131/jvsj.49.610.

[53] D. Menzel, R. Gomer, Desorption from metal surfaces by low-energy electrons, J. Chem. Phys. 41 (11) (1964) 3311–3328, https://doi.org/10.1063/1.1725730.

[54] P.A. Redhead, Interaction of slow electrons with chemisorbed oxygen, Can. J. Phys. 42 (5) (1964) 886–905, https://doi.org/10.1139/p64-083.

[55] P.A. Redhead, The first 50 years of electron stimulated desorption (1918-1968), Vacuum 48 (6) (1997) 585–596, https://doi.org/10.1016/S0042-207X(97)00030-4.

[56] F. Billard, N. Hilleret, G. Vorlaufer, Some results on the electron induced desorption yield of OFHC copper. Vacuum Technical Note 00-32, CERN, 2000.

[57] O.B. Malyshev, Vacuum in Particle Accelerators: Modelling, Design and Operation of Beam Vacuum Systems, John Wiley & Sons, 2020, https://doi.org/10.1002/9783527809134.

[58] V.V. Anashin, O.B. Malyshev, I.R. Collins, O. Gröbner, Photon-stimulated desorption and the effect of cracking of condensed molecules in a cryogenic vacuum system, Vacuum 60 (1–2) (2001) 15–24, https://doi.org/10.1016/S0042-207X(00)00239-6.

[59] R. Cimino, I.R. Collins, Vacuum chamber surface electronic properties influencing electron cloud phenomena, Appl. Surf. Sci. 235 (1–2) (2004) 231–235, https://doi.org/10.1016/j.apsusc.2004.05.270.

[60] M.H. Achard, Desorption des gaz induite par des electrons et des ions de l'acier inoxydable, du cuivre OFHC, du titane et de l'aluminium purs, CERN-ISR-VA-76-34, CERN, Geneva, Switzerland, 1976. CM-P00064839. URL: cds.cern.ch/record/314507.

[61] K. Kennedy, Electron Stimulated Desorption Rates from Candidate Vacuum Chamber Surfaces, LBL, Berkeley, July 1986.

[62] A.N. Hannah, P. Krkotič, R. Valizadeh, O.B. Malyshev, et al., Characterisation of copper and stainless steel surfaces treated with laser ablation surface engineering, Vacuum 189 (2021), 110210, https://doi.org/10.1016/j.vacuum.2021.110210.

[63] M. Haubner, V. Baglin, B. Henrist, Collector-based measurement of gas desorption and secondary electron emission induced by 0–1.4 keV electrons from LHC-grade copper at 15 K, Nucl. Instrum. Methods Phys. Res. Sect. B Beam Interact. Mater. Atoms 531 (2022) 34–43, https://doi.org/10.1016/j.nimb.2022.09.013. In press.